



Extended Ischemic Recovery After Implantation of Human Mesenchymal Stem Cell Aggregates Indicated by Sodium MRI at 21.1 T

Shannon Helsper^{1,2} · F. Andrew Bagdasarian^{1,2} · Xuegang Yuan² · Kaya Xu³ · Jea-Young Lee³ · Jens T. Rosenberg¹ · Cesario V. Borlongan³ · Teng Ma² · Samuel C. Grant^{1,2}

Received: 10 August 2021 / Revised: 17 November 2021 / Accepted: 12 December 2021
© The Author(s), under exclusive licence to Springer Science+Business Media, LLC, part of Springer Nature 2022

Abstract

Extended therapeutic application remains a significant issue in the use of stem cell therapies to treat ischemic stroke. Along these lines, neurological recovery in a rodent model of ischemic stroke was evaluated following implantation of human mesenchymal stem cell aggregates (hMSC-agg), labeled with micron-sized particles of iron oxide, directly into the lateral ventricle contralateral to the ischemic lesion hemisphere. Longitudinally, disease progression and response to hMSC-agg therapy were assessed by ¹H and ²³Na magnetic resonance imaging (MRI) at 21.1 T to investigate cellular localization, migration, and recovery over an extended timeframe. MRI provides quantifiable metrics of tissue status through sodium distributions in addition to traditional proton imaging. Quantitative ²³Na MRI revealed a significant decrease of sodium concentrations following hMSC aggregate implantation, indicating recovery of homeostasis. This result correlates positively with extended neurological recovery assessed by behavioral analysis and immunohistochemistry. These findings demonstrate the potential of implanted hMSC aggregate therapy to provide extended treatment for ischemic stroke, as well as the robustness of MRI for monitoring such approaches. This method potentially can be translated to a clinical setting for the assessment of extended cell therapy efficacy.

Keywords Magnetic resonance imaging · Sodium · Stem cells · Ischemic stroke · Preconditioning

Introduction

Stroke is a leading cause of long-term disability. Annually, nearly 800,000 people in the USA suffer a stroke and approximately 17% of the cases result in death [1]. Only one drug, tissue plasminogen activator, is clinically available, but it exhibits a narrow therapeutic window that benefits only 5% of patients [2], highlighting the need for more

effective and encompassing therapies. Although surgical interventions such as mechanical thrombectomy can extend this therapeutic window out to 12 h, these approaches still would benefit from follow-up therapy to support revascularization and neural protection in the penumbra. During an ischemic event, restricted blood flow leads to oxygen and glucose deprivation, compromised ATP production, major dysregulation of the Na⁺/K⁺-ATPase, anaerobic glycolysis, and acidosis [3–5]. A cascade of disrupted ionic homeostasis and osmotic swelling culminates in an elevated intracellular sodium concentration, excessive water influx, and neuronal death. Sodium, as a quantifiable metric of ischemic lesion and tissue recovery, is linked directly to disrupted Na⁺/K⁺-ATPase, both in the acute phase and in sub-acute and extended period after the initial injury [6].

Human mesenchymal stem cells (hMSC) have shown therapeutic effects following neurological damage and are a promising approach to minimize these acute and chronic effects [7]. Therapeutic application of hMSC in rodent models has shown to induce angiogenesis in ischemic stroke [8, 9], resulting in elevated levels of vascular endothelial

Shannon Helsper and F. Andrew Bagdasarian contributed equally to this work.

✉ Samuel C. Grant
grant@magnet.fsu.edu

¹ National High Magnetic Field Laboratory, Florida State University, Tallahassee, FL, USA

² Chemical and Biomedical Engineering, FAMU-FSU College of Engineering, Florida State University, Tallahassee, FL, USA

³ Center of Excellence for Aging and Brain Repair, University of South Florida, Tampa, FL, USA

growth factor, as well as improved functional and neurological behavior [10–13]. MSC also promote neural circuit regeneration following an ischemic event, either through promoting reorganization or recruitment of endogenous neural progenitor cells (NPC) [11, 14, 15]. Following delayed hMSC treatment, significant reduction in tissue loss has been observed, as well as promotion of endogenous neural regeneration resulting from NPC recruitment in the subventricular zone [9]. These later effects appear to be dominant, with several preconditioning culture methods employed to prepare hMSC for administration [16].

To date, most studies and clinical trials have evaluated single cell suspensions of hMSC in the treatment of stroke [17]. Single cell suspension treatments, however, can be compromised by ischemic conditions and inflammatory stress [18], resulting in low graft survival. As a result, dissociated hMSC cell suspensions may not provide extended impacts in ischemic recovery. To combat these effects and improve both engraftment, permanence, and therapeutic benefits, preconditioning of monolayer culture of hMSC under hypoxia (2.5–5% oxygen) has been shown to enhance neurogenesis as compared to normoxic culture [19] with particular upregulation of neurotrophic factors integral to neural circuit development [20]. Also, culture of three-dimensional aggregates of hMSC has demonstrated improved viability within ischemic environments [21–23]. Physiological benefits of 3D aggregation include reduced cell size as well as increased therapeutic cytokine secretion [21, 24] and migration capabilities in vitro [21, 25], features critical for enhancing the potential of cellular therapy applied to stroke. Aggregation of hMSC may prove to be an effective alternative to preconditioning methods utilizing serum from ischemic donors to induce cell modifications [26]. To date, 3D aggregates are still dissociated to single cell suspensions just prior to their administration so that vascular or intracerebral delivery can be achieved.

Tracking of implantation, retention, and quantification of therapeutic effects is essential to optimize novel cellular treatments. Here, magnetic resonance imaging (MRI) provides a unique advantage over traditional histological methods of longitudinal assessment [27]. Using intracellular contrast agents such as micron-sized particles of iron oxide (MPIO), MRI enables in vivo visualization and tracking of cells [28]. In stroke models, MRI also provides accurate in vivo measurements of lesion volume and enables in vivo assessment of tissue recovery from the evolution of proton (^1H) and sodium (^{23}Na) signal intensities [4, 11, 29–31].

In this study, to extend the therapeutic window of their application, hMSC aggregates (hMSC-agg) were transplanted intracerebroventricularly in a rat model of ischemic stroke, contralateral to the infarct or in the corresponding ventricle of naïve rats subjected to a sham surgery. Visualization of transplanted hMSC-agg was performed via MRI

at 21.1 T and combined with subsequent functional characterization of the implanted grafts using stroke-sensitive behavioral assessments and immunohistochemical assays. High-resolution ^1H fast spin-echo (FSE) and 3D ^{23}Na gradient-recalled echo (GRE) imaging on days 1, 3, and 7 post-surgery enabled tracking of lesion recovery, cell dissociation, and evolution of intracellular sodium concentrations. hMSC-agg-administered ischemic rats demonstrated recovery of sodium homeostasis with significant lesion volume reduction. Behavioral and immunohistochemical assessment confirmed hMSC-agg treatment induced functional recovery from the transient ischemic insult.

Methods

Cell Culture, Aggregation, and Characterization

hMSC were acquired from the Tulane Center for Stem Cell Research and Regenerative Medicine at Passage 3. Cells were expanded and maintained in complete culture media (CCM) containing α -MEM supplemented with 10% FBS (Atlanta Biologicals, Lawrenceville, GA) and 1% penicillin/streptomycin (Life Technologies, Carlsbad, CA) in a standard CO_2 incubator (37 °C and 5% CO_2), with media changes every 3 days. Cells were grown to 70–80% confluence and then harvested by incubation with 0.25% trypsin/EDTA (Invitrogen) for 5 min in a standard CO_2 incubator. Harvested cells were re-plated at a density of 2,000 cells/cm² and sub-cultured up to Passage 5. hMSC then were exposed to 1.80-, 0.90-, or 0.45- $\mu\text{g}/\text{mL}$ MPIO contrast agent labeled with a green fluorophore (BANGS Laboratories, Inc. Fishers, IN) for 12 h. After labeling, hMSC were washed with phosphate-buffered saline (PBS) to remove extra MPIO, and 5,000 cells in 200- μL culture medium were added to each well of an ultra-low attachment (ULA) 96-well plate with a round bottom (Corning, Corning, NY) for aggregation. hMSC-agg were cultured for 48 h, then washed with PBS, and suspended in 50–100 μL PBS for transplantation. *For in vivo* administration, the 1.80- $\mu\text{g}/\text{mL}$ MPIO concentration was used. All culture reagents and chemicals were purchased from Sigma-Aldrich (St. Louis, MO) unless otherwise noted.

In order to assess inflammatory action in vitro, indoleamine 2,3-dioxygenase (IDO) enzymatic activity, including both IDO1 and IDO2, was determined by kynurenine level in cell culture supernatant as described previously [24, 32]. Briefly, a 400- μL supernatant from hMSC culture was mixed with trichloroacetic acid (200 μL , 30% by weight), followed by centrifugation at 8,000 g for 10 min. An equal volume of Ehrlich reagent (2% p-dimethylaminobenzaldehyde in glacial acetic acid) was added to the supernatant, and optical density at 490 nm was measured with an iMark™ microplate reader (BioRad, Hercules, CA). In addition, cell viability in

each aggregate was determined by PicoGreen DNA assay (Life Technologies, Carlsbad, CA) as described previously [21].

Animal Model

All animal procedures were completed in accordance with the Animal Care and Use Committee at the Florida State University. All studies were conducted in accordance with the United States Public Health Service's Policy on Humane Care and Use of Laboratory Animals as well as the US NIH Guide for the Care and Use of Laboratory Animals (NIH Publications, No. 8023, 1978 revision). Transient middle cerebral artery occlusion (MCAO) was instituted for 1.5 h following techniques previously established [33, 34]. Briefly, a rubber-coated filament (Doccol Corp., Sharon, MA) was inserted into the external carotid artery and threaded 1.9 cm into the internal carotid artery to block the circle of Willis, effectively occluding the MCA. Eighteen male Sprague–Dawley rats weighing between 200 and 250 g (Envigo, Indianapolis, IN) underwent either MCAO or a sham surgery involving tissue dissection to the MCA to mimic post-operative conditions. Immediately following filament removal, rats were secured in a stereotaxic instrument and administered an intracerebral ventricular (ICV) injection based on coordinates from bregma. Each received either 20 MPIO-labeled hMSC-agg suspend in 50- μ L saline or control saline vehicle only, resulting in the following randomly assigned groups: ischemic with hMSC-agg (MCAO + Agg; $n = 6$), ischemic with vehicle (MCAO + vehicle; $n = 7$), or sham with hMSC-agg (Sham + Agg; $n = 5$). Rats were induced with 4–5% isoflurane in 100% O₂ and maintained at ~3% anesthesia for the duration of surgery. All individuals received pre- and post-operative analgesics (bupivacaine and buprenorphine, respectively) as well as saline for rehydration, with additional administration as needed post-operatively. Additionally, animals recovered in a warmed incubator before returning to their home cages. Baseline behavioral assessments were conducted with subsequent testing on days 3 and 7 post-surgery corresponding to MR on days 1, 3, and 7. Following scans, the animals were perfused transcardially with 4% paraformaldehyde for ex vivo MRI and excised brains placed in 30% sucrose prior to sectioning for immunohistochemistry (IHC).

In Vivo Magnetic Resonance Imaging

All in vivo scans were performed at the 21.1-T, 900-MHz vertical MRI scanner [35] at the National High Magnetic Field in Tallahassee, Florida. The magnet was equipped with a Bruker Avance III console and scans were recorded using Paravision 5.1 (Bruker, Inc., Billerica, Massachusetts). Rats were loaded into a home-built linear birdcage double-tuned

²³Na/¹H radio frequency coil tuned to 237 and 900 MHz, respectively. All rats were oriented in a supine position within the cradle and maintained at or below 3% isoflurane during imaging to ensure a steady respiration rate while in the magnet. Respiration was monitored (Small Animal Instruments, Inc., Stony Brook, New York) and used for acquisition triggering during MRI.

Localization images in the axial, coronal, and sagittal planes utilized a ¹H rapid acquisition with relaxation enhancement (RARE) sequence. All high-resolution ¹H images were acquired in the anatomical coronal orientation with 35 slices, each 0.5 mm thick, extending from the mid-hippocampus to olfactory bulb. T₂-weighted images were generated utilizing a ¹H 2D FSE sequence with 100 × 100 μ m in-plane resolution [effective TE = 25 ms, TR = 6000 ms] to measure ischemic lesion volumes. Aggregate localization within the ventricular system and cell dissociation were assessed using a 2D GRE sequence with 50 × 50 μ m in-plane resolution and two averages [TE = 4 ms, TR = 1000 ms]. For sodium acquisitions, a ²³Na 3D GRE imaging sequence was used to yield (1.6-mm)³ isotropic resolution in one average [TE = 0.700 ms, TR = 60 ms].

Ex Vivo Magnetic Resonance Imaging Protocol

Prior to ex vivo imaging, perfused brains were excised after day 7 post-MCAO and washed in PBS for 48 h. Brains were immersed in Fluorinert (3 M Corp, Minneapolis, Minnesota) for 24 h to minimize susceptibility artifacts [36] prior to imaging in a 15-mm NMR tube. Ex vivo images were acquired at (50- μ m)³ isotropic resolution [TE = 7.5 ms, TR = 150 ms] using a ¹H 3D GRE sequence at 11.75 T to assess cell dissociation from implanted aggregates.

Image Analysis

Raw data was reconstructed and analyzed without filtering using AMIRA 3D visualization and analysis software (Thermo Fisher Scientific, Waltham, Massachusetts). Ischemic lesions were delineated via thresholding defined by hemispheric contralateral signal and standard deviation on day 1 post-surgery for ¹H FSE (*threshold* = +1 Std. Dev.) and ²³Na GRE (*threshold* = +2.5 Std. Dev.). Signal threshold on the ipsilateral side for both scan sets was determined according to:

$$S_{\text{ipsilateral}} = S_{\text{contralateral}} + \text{threshold} \quad (1)$$

Signals exceeding the defined values were selected as part of the ischemic region. Calculated volumes were normalized to day 1 to obtain fractional changes for days 3 and 7. Proton and sodium volume and signal intensity within ischemic

lesions were assessed for early (days 1 to 3) and late (days 1 to 7) period after treatment.

hMSC-agg localization and cellular dissociation were determined using a pre-determined maximum signal threshold and anatomical reference to discern MPIO contrast from artifacts and other hypo-intense signals (i.e., blood vessels, injection site). Both ^1H in vivo GRE and 3D ex vivo scans were analyzed. The MPIO intracellular label induced an 81.7% decrease in proton signal in the hMSC specimens as compared to the maximum signal. This reduction was used to define the threshold for in vivo cell volume measurements. Ex vivo data were processed by subtracting images of the entire brain with and without void volumes, including the injection site, providing an estimate of MPIO label volume.

Behavioral Tests

Behavioral tests were completed on all animals prior to imaging (days 1, 3, and 7). The behavioral test groups included one more animal as compared to the imaging groups. For these extra animals, only the initial stroke size and successful cell injection were confirmed using MRI. The cylinder test previously described [37, 38] was used to assign each animal a spontaneous forelimb usage asymmetry score at day 0 (baseline) pre-surgery and days 3 and 7 post-surgery. Rats were placed in a tall transparent vertical cylinder for 10 min. The number of independent forepaw contacts with the cylinder surface was recorded. Fractional usage of the unimpaired ipsilateral (I) forelimb to that of the impaired contralateral (C) forelimb was calculated according to:

$$\text{Limb Use Asymmetry Score} = \frac{I}{I + C + B} - \frac{C}{I + C + B} \quad (2)$$

Occasions when both (B) forelimbs were used simultaneously also were considered. A positive score indicates unimpaired preference while scores close to zero indicate near-symmetric forelimb usage. The elevated plus maze was used to measure anxiety and recovery [39]. The maze is constructed as two open and two enclosed arms elevated 52 cm off the floor. Rats were placed in the center of the elevated plus maze facing one of the open arms and recorded with a camera for 5 min. The number of open arm entries and total time spent in the open arms were recorded as a measure of stress. Additionally, the open field test was used to assess vertical and horizontal locomotion discrepancies and stress [40–42]. Rats were placed in the center of an open field with dimensions $92 \times 92 \times 56$ cm and an equally distributed 36 square grid for 10 min. Total distance traveled was measured to indicate locomotive activity. Additionally, time spent within the grid center compared to exterior was determined as a measure of stress.

Immunohistochemistry

Following ex vivo imaging, excised brains were washed in PBS and immersed in 30% sucrose. Histological stains were performed to analyze therapeutic retention and tissue regeneration. hMSC were localized via HuNu staining to visualize human cell nuclei. Astroglial activation and gliosis during neurodegeneration were measured with anti-gial fibrillary acidic protein (GFAP) antibody. Additionally, doublecortin (DCX) staining provided evaluation of neurogenesis and neuronal migratory patterns for newly developed neurons while NeuN staining tagged mature neurons specifically. Finally, DAPI was used as counter-staining.

Statistical Analysis

All MRI measurements and behavioral test results were statistically analyzed using JMP 14 software for Windows (SAS Institute, Cary, North Carolina), applying the MANOVA model for repeated measures, followed by a Tukey's highly significant difference post hoc test between groups, to determine significance ($p < 0.05$). IHC results were calculated by a one-way ANOVA analysis followed by Bonferroni's multiple comparison test. For all statistical analyses, $*p < 0.05$, $**p < 0.01$, $***p < 0.001$. Mean values and standard error of the mean have been included for all IHC figures.

Results

In Vitro Characterization of hMSC Aggregates

To determine optimal dosage of the labeling agent, hMSC aggregates were labeled with MPIO contrast agent at different concentrations (1.80, 0.90, or 0.45 $\mu\text{g}/\text{mL}$) and imaged using MRI. MPIO labeling slightly increased hMSC-agg size and decreased compaction as compared to control aggregates. However, there was no significant difference in these measures between MPIO concentrations (Fig. 1a–c), and hMSC viability was not influenced by MPIO labeling (Fig. 1d). As shown in Fig. 1e, aggregation of hMSC significantly improved the immunomodulatory potential. When re-plating hMSC-agg on tissue culture surfaces, hMSC carrying MPIO agents successfully migrated out from the aggregate (Fig. 1f). By ex vivo MRI, concentration of MPIO was optimized to label hMSC and form aggregates (Fig. 1g).

In Vivo MRI

All hMSC applied in in vivo transplantation were labeled using 1.80- $\mu\text{g}/\text{mL}$ MPIO. Aggregate localization, migration, cellular dissociation, and ischemic lesion volume were assessed on days 1, 3, and 7 post-surgery/cell transplantation

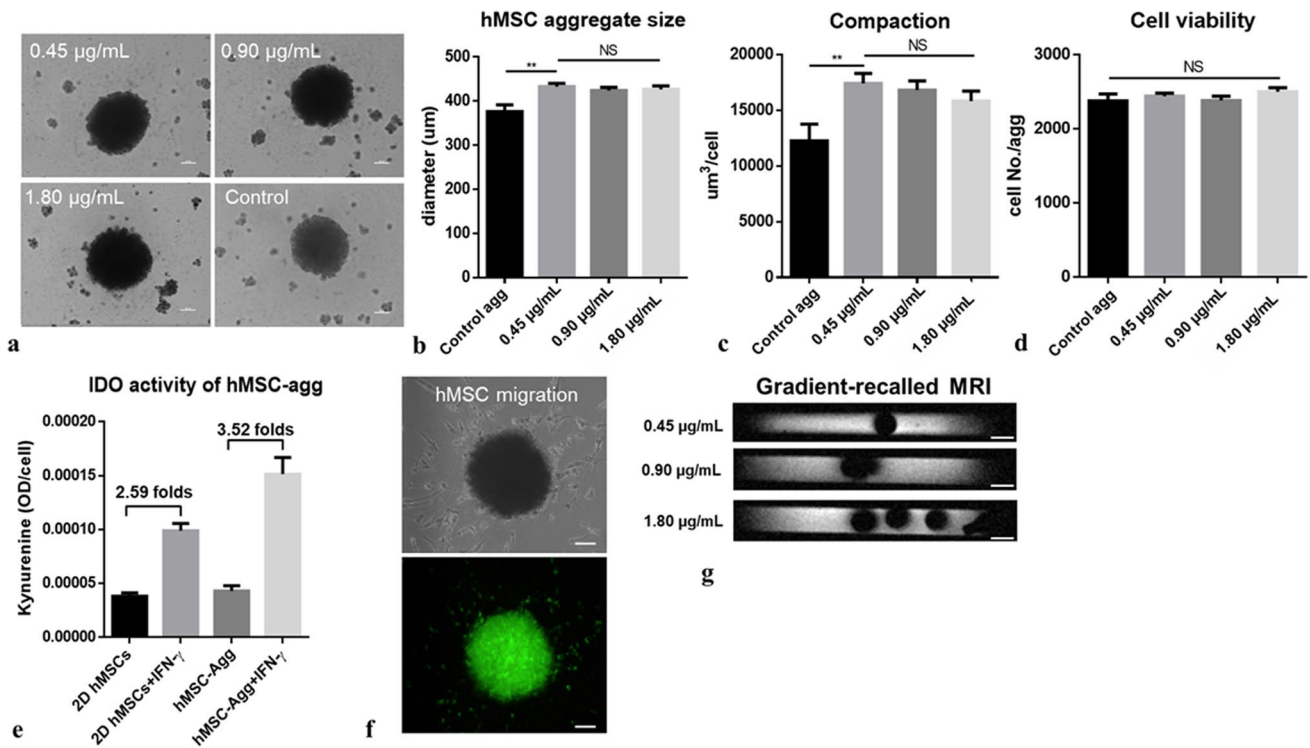


Fig. 1 Characterization of hMSC aggregates (hMSC-agg) with MPIO labeling. **a** Microscopy images of hMSC-agg labeled with 1.80-, 0.90-, or 0.45-µg/mL MPIO contrast agent. Scale bar=100 µm. **b** Aggregate size and **c** compaction analysis of hMSC-agg labeled with different concentration of MPIO. **d** Cell viability of hMSC within aggregates labeled with different concentrations. **e** IDO activi-

ty of hMSC-agg compared to monolayer cultured hMSC. **f** Microscopy images of cell migration from hMSC-agg labeled with 0.45-µg/mL MPIO. Scale bar=100 µm. **g** Ex vivo GRE scan at 11.75 T (TE=16.1 ms, TR=500–1500 ms) of hMSC-agg labeled with different concentrations of MPIO. Scale bar=50 µm. All values presented as mean ± SD (***p* < 0.01, one-way ANOVA, Tukey post hoc test)

using ¹H and ²³Na MRI. In vivo ¹H GRE scans demonstrated successful aggregate implantation with prolonged retention of MPIO-labeled aggregates out to day 7 (Fig. 2) prior to sacrifice, providing evidence of extended permanence and potential extended action in the ischemic brain.

Hyperintense ¹H signal in T₂W images corresponding to the ischemic lesion decreased longitudinally on days 3 and 7 post-surgery (Fig. 3). On day 3, the vehicle group

exhibited a volume increase and high standard deviations in their fractional volume changes. After 7 days, average ¹H volume decreased by 55.2% in the treated ischemic group compared to 16.1% in the vehicle-injected group. By contrast, the hMSC-Agg-treated ischemic group exhibited a decrease in lesion volume in both early and late time periods, though still with high standard deviations.

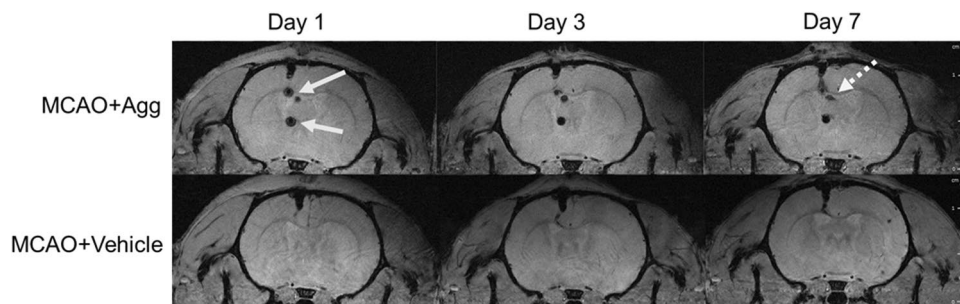


Fig. 2 Localization of aggregates (bold arrows) within the ventricular system of hMSC-agg-administered ischemic rats is visualized on days 1–7. Potential cell dissociation on day 7 (dotted arrow) was assessed in vivo utilizing a ¹H GRE sequence (50×50×500 µm; TE=4 ms,

TR=1 s). Successful therapy implantation into the contralateral hemisphere was achieved with prolonged retention of MPIO-labeled bodies at the implantation site out to day 7

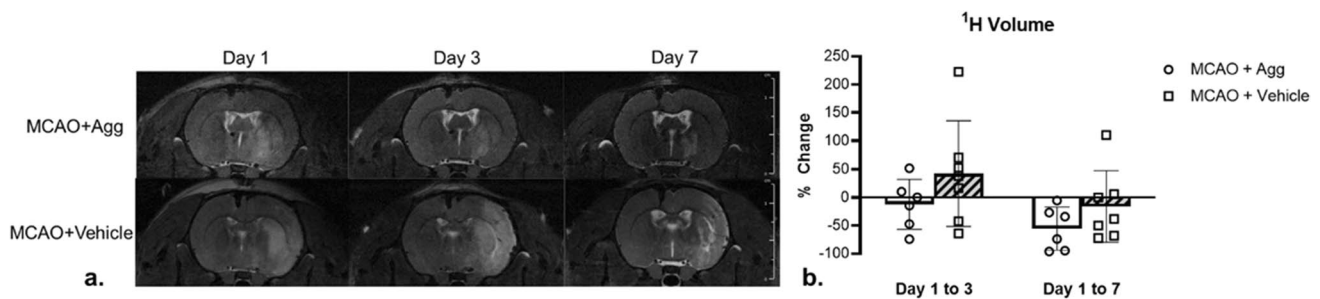


Fig. 3 **a** T_2W 1H FSE images ($100 \times 100 \mu m$, $TE=25$ ms, $TR=6$ s) demonstrated cortical and striatal hyperintense signal indicative of the ischemic lesion over 7 days. **b** A longitudinal reduction in lesion volume calculated based on 1H signal (Eq. 1) is observed for both MCAO groups with fragmentation of the ischemic lesion seen on

day 7. An initial increase in lesion volume, indicated by positive percent change, was seen on day 3 for the MCAO+vehicle group only. However, neither group demonstrated significant decrease in lesion volume between day 1 and 3 or day 1 and 7 according to Eq. 1. All values presented as mean \pm SD

Fragmentation of the stroke nevertheless remained observable for both ischemic groups.

^{23}Na 3D GRE imaging provides improved metrics for studying the mechanisms of ischemic stroke recovery as compared to conventional 1H T_2W methods. Evaluated with ^{23}Na 3D GRE imaging, lesion volume significantly decreased from day 1 to 7 in the treated ischemic group compared to vehicle only ($p=0.0106$). Figure 4 demonstrates representative images from each group longitudinally; slices are matched to 1H T_2W images seen in Fig. 3 for anatomical reference. On average, the treatment group decreased 36.1% in the lesion volume whereas vehicle-injected group volumes increased 6.4%, indicative of ionic homeostatic recovery with hMSC-agg implantation (Fig. 4b). hMSC-agg-treated subjects consistently decreased in lesion volume over the 7-day time course. In contrast, vehicle-administered subjects exhibited sporadic changes in ischemic volume, with an average increase in fractional volume change on day 3 as illustrated in Fig. 5. Concomitantly, a greater degree of

sodium volume reduction was seen in the later time period for hMSC-agg-implanted ischemic animals as indicated by comparison between fractional changes for days 1 to 7 and 1 to 3 ($p=0.0028$). Signal intensity within the lesions demonstrated similar trends as volumetric measurements (Suppl. Fig. S1).

Ex Vivo MRI and IHC

Aggregate retention and cell dissociation from aggregates were confirmed by ex vivo 3D GRE data and IHC. Dissociated cell migration from hMSC-agg along the corpus callosum and throughout the ventricular system was evident from the high-resolution ex vivo images shown in Fig. 6. The expansion of cellular aggregates was determined volumetrically on ex vivo MR data, enabling comparison of sham and ischemic animals ($p>0.05$).

Although migration towards the ischemic lesion was minimal, co-localization of human cell marker (HuNu) and

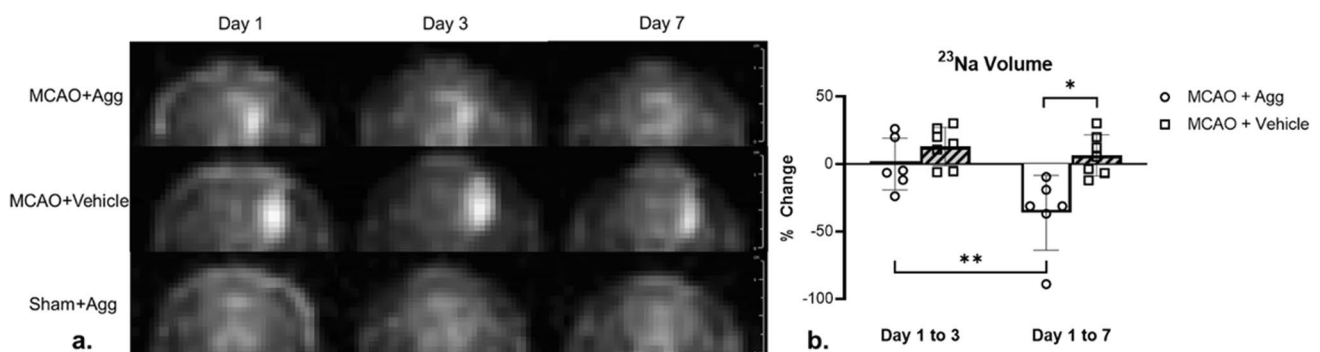


Fig. 4 **a** Recovery of sodium homeostasis, evaluated via ^{23}Na GRE at 1.6-mm isotropic resolution ($TE=0.7$ ms, $TR=60$ ms). Slices are matched to 1H T_2W -weighted images seen in Fig. 3 for anatomical reference. Ischemic lesion volume, calculated according to Eq. 1 from ^{23}Na signal, decreases longitudinally in MCAO+Agg animals as

compared to the MCAO+vehicle group; Sham+Agg were used as a control. **b** Evolution of the fractional change of the ischemic lesion volume as compared to day 1 (** $p=0.0028$, * $p=0.0106$, repeated measures MANOVA, Tukey post hoc test). All values presented as mean \pm SD

Fig. 5 Average ischemic lesion volumes (mean \pm SD) indicated for MCAO + Agg (top) and MCAO + vehicle (bottom) groups assessed via ^{23}Na GRE as well as ^1H T₂W images. 3D renderings present median lesion volumes and extents for each cohort and time point. Scale bar = 5 mm

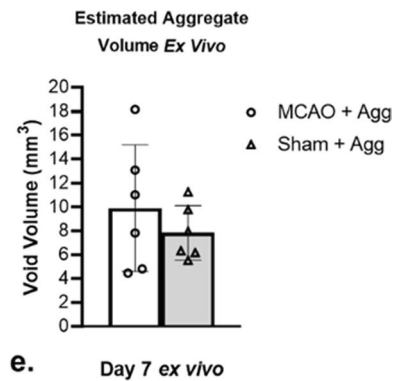
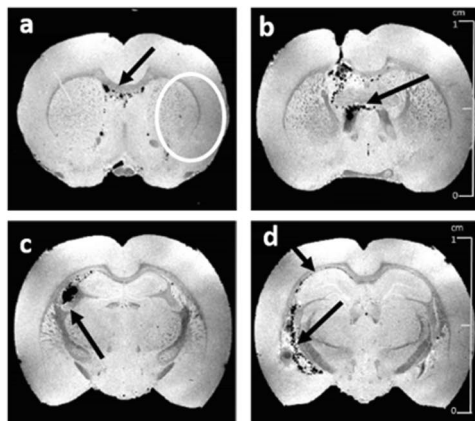
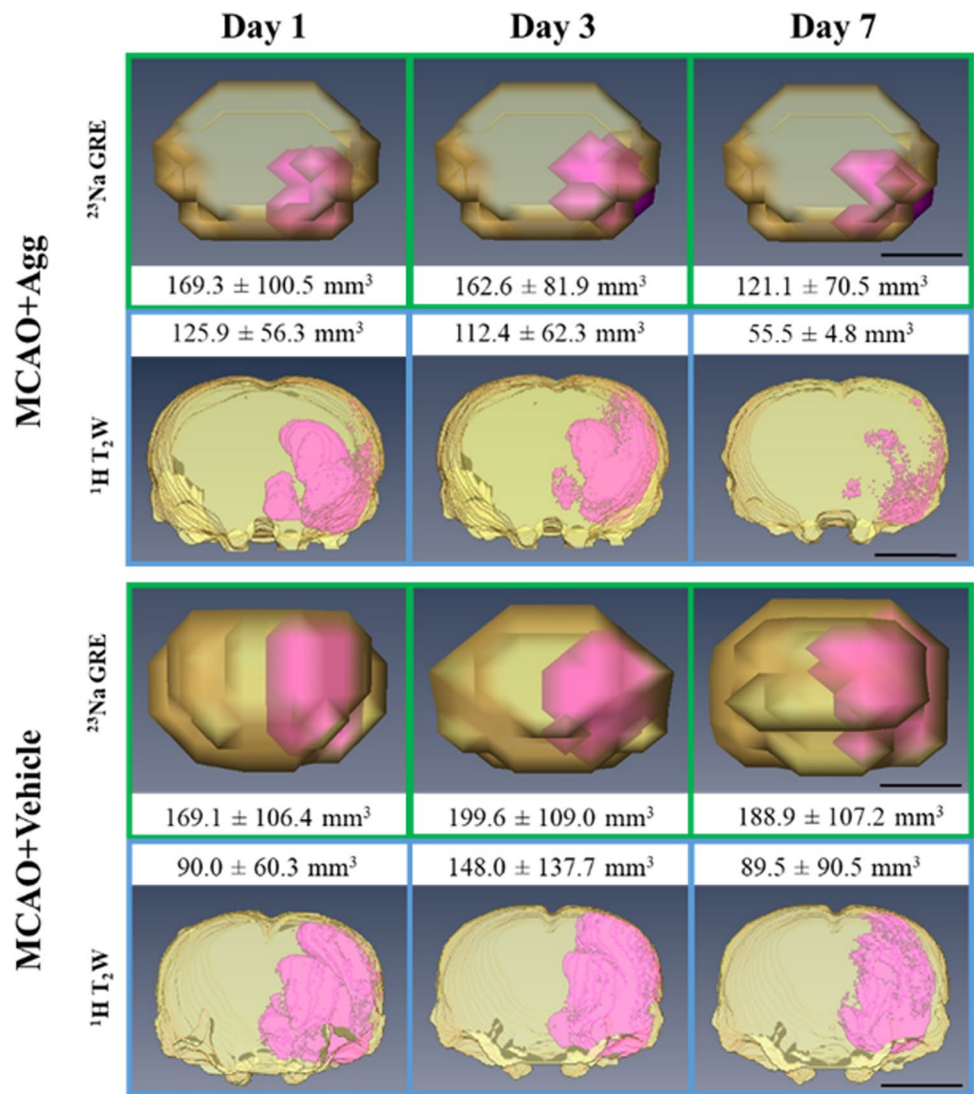


Fig. 6 3D ex vivo GRE images (50- μm isotropic; TE=7.5 ms, TR=150 ms) were acquired at 11.75 T to assess cell dissociation 7-day post-implantation. **a–d** A representative MCAO+Agg specimen showing neuro-anatomical regions progressing anterior to pos-

terior with localization of MPIO visualized by signal voids (arrows) relative to the location of the ischemic lesion (circle). **e** Similar total cell volumes are calculated for both MCAO+Agg and Sham+Agg groups. All values presented as mean \pm SD

MPIO green fluorophore (Fig. 7) support cellular dissociation and migration from aggregates seen in ex vivo MR images. Levels of HuNu staining associated with human cell marker were elevated in ischemic rats as compared to sham with hMSC-agg ($p < 0.05$). Significant differences in staining for GFAP were observed between all three groups ($p < 0.001$). The vehicle-injected ischemic group demonstrated the highest levels of GFAP staining followed by treated ischemic and finally sham groups. Neuronal staining in treated ischemic animals exhibited significantly higher levels of DCX stain indicative of neuronal migration, compared to both other groups ($p < 0.05$). Furthermore, elevated levels of NeuN staining were observed in sham ($p < 0.01$) and hMSC-agg-treated ischemic compared to vehicle-injected ischemic groups ($p < 0.001$). Additional sections

rostral to Fig. 7 can be found in the supplementary information (Suppl. Fig. S2 and S3).

Morphology, compaction, and density of cells along the corpus callosum also were compared between hemispheres and treatment groups using Nissl staining. Tissue recovery is evident in hMSC-agg-treated ischemic animals compared to those administered vehicle only (Fig. 8).

Behavioral assessments

The cylinder test demonstrated significant decrease in symmetry for the vehicle-injected ischemic group on days 3 ($p = 0.0216$) and 7 ($p = 0.0122$) as compared to baseline (Fig. 9). However, a near zero spontaneous forelimb usage asymmetry score was evident for the treated ischemic group

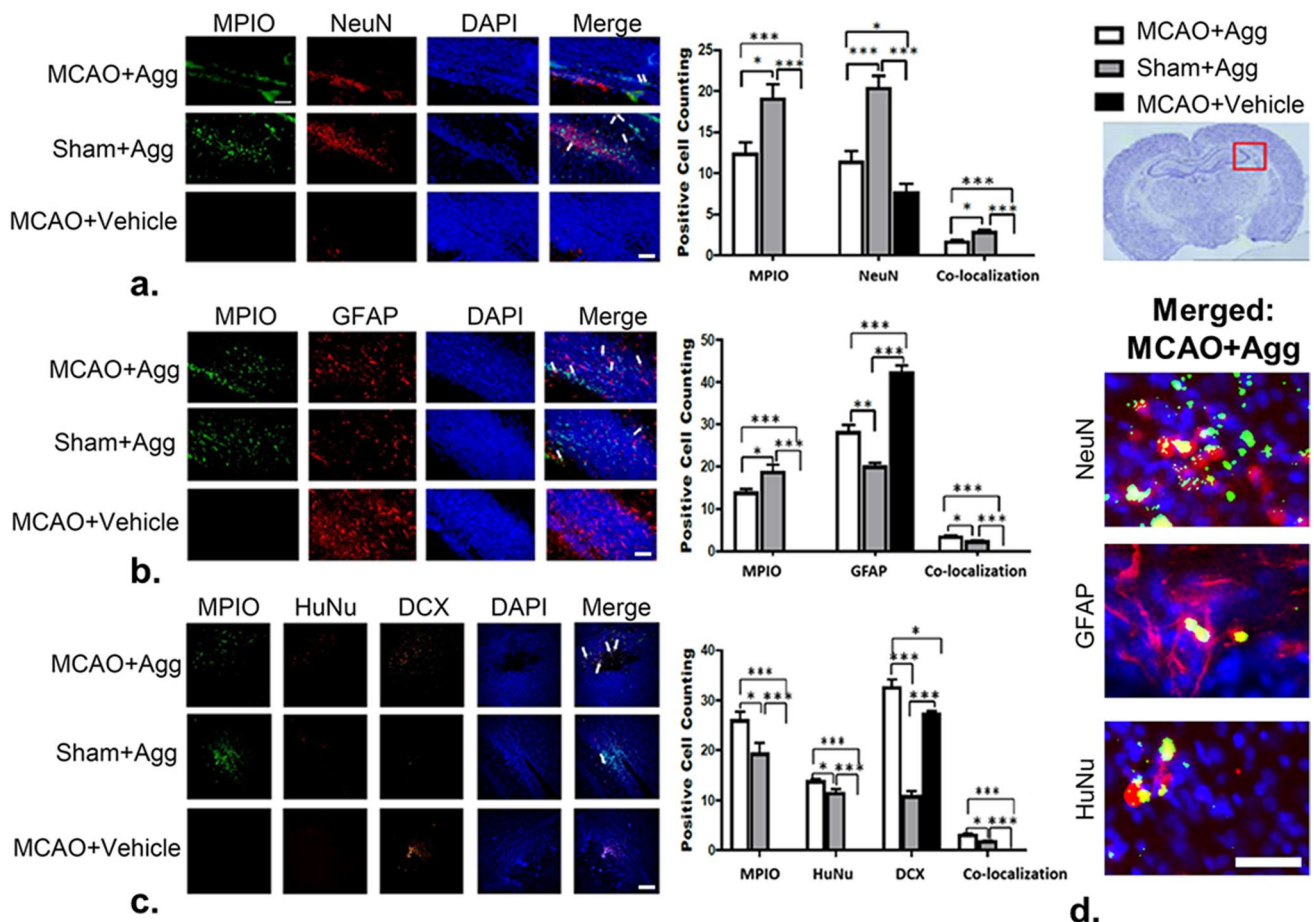


Fig. 7 IHC indicating tissue recovery correlates with MRI and behavioral assessments. Red boxes in the representative Nissl sections demonstrate location of magnified regions. Areas of co-localization indicated by stain overlap are highlighted by white arrows in the merged column. **a** Significantly increased NeuN staining for mature neurons in hMSC-agg-implanted animals supports neuroprotection ($p < 0.05$). **b** Significantly elevated GFAP staining in MCAO+vehicle ($p < 0.05$) suggests increased and prolonged astrocytic activity in response to tissue damage [42] compared to MCAO+Agg. **c** Co-

localization of HuNu staining with MPIO label suggests high retention of hMSC-agg in cerebral tissue. Furthermore, elevated levels of DCX stain in MCAO+Agg indicate increased neurogenesis and NPC migration. **d** Magnified images of merged panels for MCAO+Agg taken from highlighted regions (white arrows) in panels (a–c). Scale bars = 50 μ m. All values presented as mean \pm SEM ($*p < 0.05$, $**p < 0.01$, and $***p < 0.001$, one-way ANOVA, analysis Bonferroni's multiple comparison)

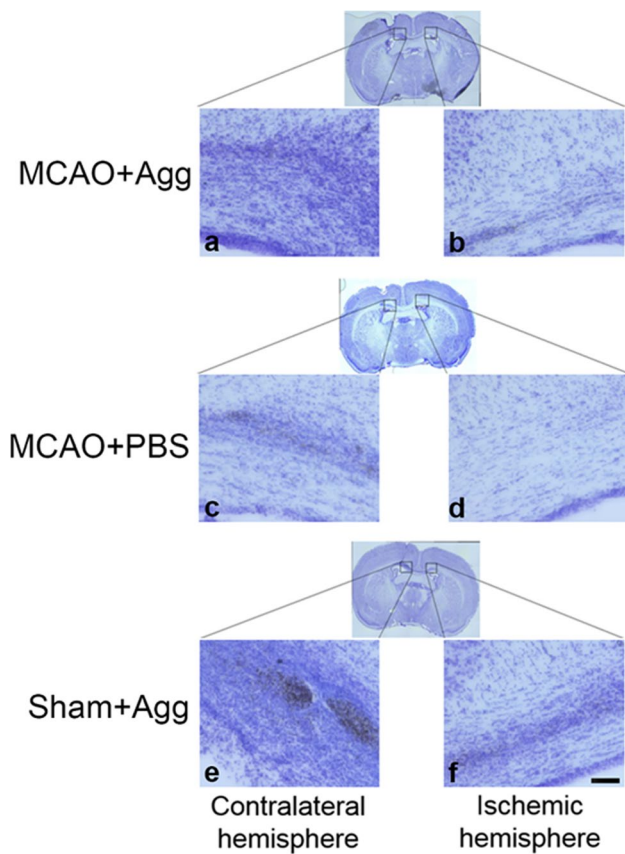


Fig. 8 Representative slices of Nissl staining focused on the corpus callosum in both the ischemic and contralateral hemispheres for **a, b** MCAO+Agg; **c, d** MCAO+vehicle; and **e, f** sham+Agg. Scale bar = 100 μ m

at all time points. Comparing groups, vehicle-injected animals were significantly more asymmetric than sham animals on days 3 ($p=0.0200$) and 7 ($p=0.0136$). Importantly, no difference was observed between treated ischemic and sham with hMSC-agg groups. The elevated plus maze characterization demonstrated no statistically relevant difference for the number of open arm entries between any groups. Significant differences in total time spent in open arms were, however, observed between vehicle ischemic and sham animals on day 3 ($p=0.0329$). In contrast, hMSC-agg-treated ischemic and sham animals remained at baseline on day 3. On day 7, vehicle-injected ischemic animals returned to baseline. Neither for distance traveled during the open field test nor for duration spent in the grid center was a statistically relevant difference observed between groups over time or at individual time points.

Discussion

MPIO-labeled hMSC-agg transplanted in ischemic rats were tracked in vivo using ^1H MRI over an extended time-frame of 7 days. The necessary labeling concentration of the MPIO MR contrast agent was determined to optimize signal contrast while avoiding cytotoxicity, based on previous research [43]. As result, the MPIO contrast agent did not influence hMSC viability nor aggregate kinetics. Compared to single cell administration, aggregation permitted for a significant reduction in the required MPIO content for MRI detection [28, 44]. Initial localization of hMSC-agg via in vivo ^1H GRE scans demonstrated successful implantation into the ventricular system, as well as the prolonged and extended residence of these grafted implants in the ventricles. Although others previously have demonstrated that hMSC implanted in the contralateral hemisphere are able to migrate to the injury due to inflammatory chemokine signals [45], the majority of hMSC-agg remained in the contralateral hemisphere or within the ventricular system. Nevertheless, this robust and extended graft survival of hMSC-agg, as seen by IHC, coincided with behavioral recovery and was coupled to a reduced deleterious astrocytic activation and increased neuronal migration and survival within the ischemic region. Therefore, the graft survival likely works in tandem with other endogenous repair mechanisms through paracrine effects and stimulation of NPC. Preconditioning of hMSC has been shown to enhance therapeutic efficacy over 2D monolayer culture [46]. Specifically, 3D aggregation culture enhances hMSC migration and secretory profiles that contributed to sustained delivery of trophic and paracrine factors in stroke treatment [43, 46]. While hMSC derived from 3D aggregation culture have been shown to exhibit improved cell survival and resistance of ischemic environment, possibly due to activation of the PI3K/Akt signaling pathway [21, 23, 43], deriving single cells from 3D aggregates requires trypsinization and mechanical dissociation, which may cause low yield and cellular damage to the hMSC. Therefore, the direct use of implanted hMSC-agg has the added benefit of eliminating this cellular damage as well as extending the retention of hMSC in the ischemic brain.

3D ^{23}Na GRE scans provide quantitative measurements of the ischemic core and at-risk tissue recovery. Normalization to individual disease progression as evaluated by fractional changes in ^{23}Na signal volume over time demonstrated a significant reduction in sodium volume in the hMSC-agg-treated ischemic group as compared to controls (Fig. 4). Because a reduction of intracellular sodium levels is indicative of ionic homeostatic recovery, the present result indicates that ^{23}Na MRI can assess disease

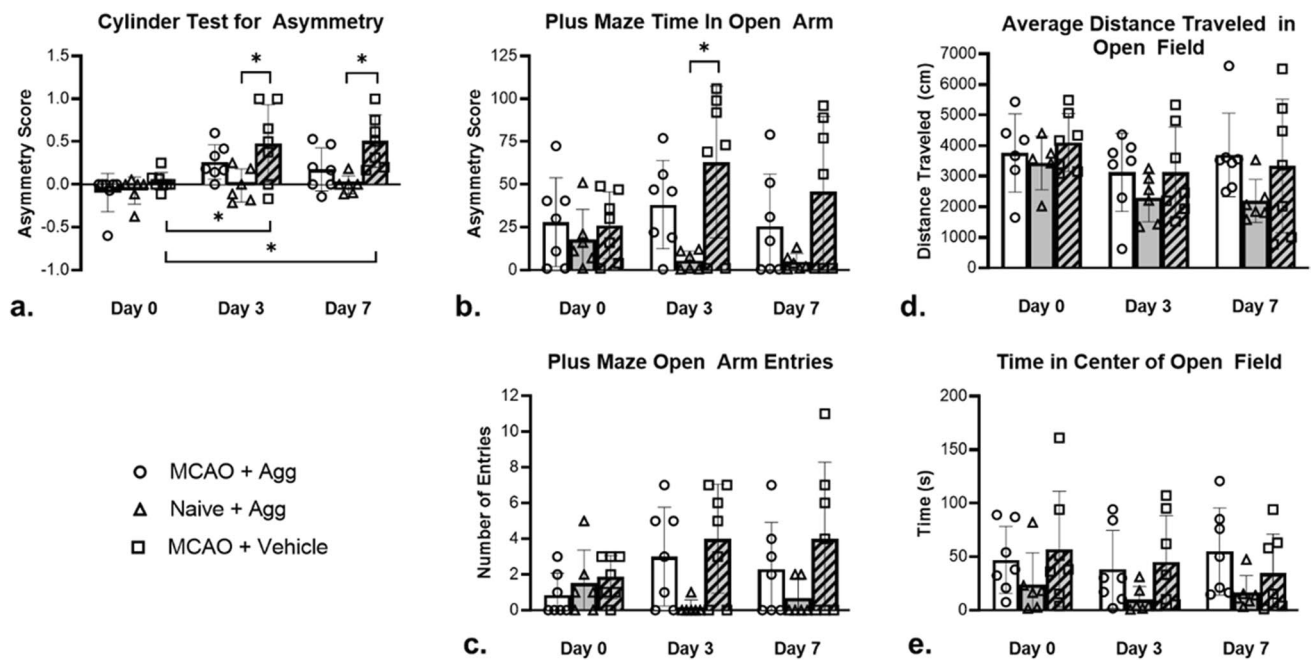


Fig. 9 Behavioral tests were performed prior to surgery (day 0) to acquire baseline measurements as well as 3- and 7-day post-surgery. **a** Asymmetry scores were calculated according to Eq. 2 utilizing the cylinder test. MCAO+vehicle animals demonstrated longitudinal increase in asymmetry on days 3 ($p=0.0268$) and 7 ($p=0.0150$). Significance was demonstrated between Sham+Agg and MCAO+vehicle on days 3 ($p=0.0200$) and 7 ($p=0.0136$). **b** Significant difference

in time spent in open arms of the plus maze between MCAO+vehicle and Sham+Agg on day 3 ($p=0.0167$) was demonstrated. **c** The number of open arm entries in the plus maze and **d** average distance traveled and **e** time in the center of the open field were also measured. All values presented as mean \pm SD (* $p < 0.05$, repeated measures MANOVA, Tukey post hoc test)

progression from quantifiable disruption and recovery of ionic equilibrium, thus providing access to a sensitive biomarker to evaluate treatment efficacy. The restoration of ATP production and Na^+/K^+ -ATPase-induced sodium homeostasis as indicated by a return towards baseline was indeed unique to hMSC-agg-treated ischemic animals. While ^1H scans did not demonstrate significance in lesion reduction, likely due to high standard deviation from signal drop-off specific to T_2W scans, decreasing volumetric trends were evident from 3D ^{23}Na GRE imaging out to day 7 for both ischemic groups. Though group assessments were performed via percent changes of ischemic volumes within individual animals, the average lesion size (mean \pm SD) and extent are demonstrated for the median 3D renderings for each group and time point in Fig. 5. This progression highlights not only the typical lesion extent, but also an average reduction in lesion size following hMSC-agg intervention apparent with both ^{23}Na and ^1H volumetrics.

Behavioral assessments of limb asymmetry demonstrated longitudinal improvement correlated with recovery of sodium homeostasis; significant improvements were identified for the treated versus vehicle-injected ischemic animals. Lack of significance between treated ischemic and sham groups indicated hMSC-agg administration contributes

to more baseline-like results in asymmetric behavior as compared to the vehicle group. Plus maze results demonstrated differences only between vehicle-injected ischemic and sham on day 3. The lack of significance on day 7 demonstrated a return towards baseline and, more importantly, the maintenance of normal anxiety levels in the hMSC-agg-treated ischemic group to an extended time point.

Ex vivo ^1H GRE imaging in combination with HuNu staining confirmed 3D hMSC-agg retention up to at least day 7. Most of the MPIO-labeled cells remained in the ventricles. The low number of MPIO-labeled or HuNu-positive cells outside the ventricle without significant ipsilateral migration suggests impacts via paracrine effects and neural progenitor action. Quantitatively, the total volume of MPIO-labeled cells confirms only minimal cellular dissociation and migration in both ischemic and sham groups administered with hMSC-agg. Long-term viability of hMSC was confirmed via co-localization with DAPI. Co-localization of human cell marker in proximity to the MPIO fluorescence supports hMSC retention within cerebral tissue, increased migration, as well as confirmation of visualized dissociated cells in ex vivo scans. Markers for both human cell and MR label were elevated in treated ischemic compared to sham animals, confirming the enhanced viability, migration, and retention

in an ischemic environment, confirming previous reports in literature [43]. The naturally induced hypoxic environment within aggregate bodies clearly contributes to the increased survival and migration by preconditioning cells to ischemia [21, 22].

GFAP, a marker of astroglial activation and gliosis during neurodegeneration, indicates the presence of a rapid and severe activation that ultimately induces inflammation and eventual scarring [47]. Thus, minimal activated GFAP expression in sham animals was expected. Elevated GFAP levels in vehicle-injected animals suggest cell death and remodeling with exacerbated astrocyte scarring within ischemia, whereas reduced GFAP levels in hMSC-agg-treated ischemic rats indicate a protective mechanism against such deleterious astrocytic response. These results are in contrast to NPC treatment-based studies [48].

Increased neurogenesis and neuronal migration evaluated by elevated DCX stain in treated versus vehicle ischemic and sham animals indicate significant and extended tissue recovery as a result of hMSC-agg treatment [49], thus confirming the disease progression indicated by ^{23}Na MRI. Increased expression of migration assisting proteins indicates higher recruitment levels due to hMSC-agg, in combination with the normal response to ischemia. Neuronal differentiation, as evaluated by NeuN [49], demonstrated longer retention of mature neurons in sham, likely as a result of non-ischemic stress. However, hMSC-agg-treated ischemic animals also indicated increased levels of retention as compared to vehicle counterparts, strongly suggesting the extended protective effect of hMSC-agg. The low co-localization of MPIO-labeled cells with increased NeuN expression provides evidence that recovery due hMSC-agg is multifaceted, relying on both the graft survival and stimulated endogenous repair mechanisms. Furthermore, these migratory and differentiation characteristics observed for hMSC-agg concur with previous findings reporting the therapeutic efficacy of MSC in general for CNS disorders, including stroke [13].

Limitations

The number of animals used in this study is low for each group; however, the power of analysis was maintained based on calculations previously determined for quantitative sodium metrics [43]. Furthermore, immediate hMSC aggregate administration may be not feasible for all clinical situations, although this method provides a positive baseline assessment of the therapeutic value of in vivo aggregate implantation. Future studies should investigate therapeutic efficacy following administration at even more extended time points after initial ischemia to establish even more clinical feasibility and extend quantitative metrics to investigate chronic response.

Conclusion

With extended permanence of the implant, the present study demonstrates recovery of sodium homeostasis and neuronal differentiation in an ischemic stroke rodent model following immediate intracerebral ventricular transplantation of large (~400 μm diameter) hMSC aggregates. Intracellular retention of the MR contrast agent is maintained through the duration of imaging as verified by ex vivo staining. This consistency supports an innate and prolonged resistance to the ischemic environment as a result of aggregation [21, 22, 25] that, with direct administration into the ventricular system, contributes to extended retention in cerebral tissue as compared to previous single cell delivery methods [43]. Further optimization and tracking of NPC from the subventricular zone to promote neural differentiation and anti-inflammatory response are desirable. Even so, evidence of NPC recruitment and overall protection of mature neurons is significantly elevated with hMSC aggregate treatment. Thus, an enhanced dose of regenerative cytokine secretions and an extended cell therapy source has been established.

Supplementary Information The online version contains supplementary material available at <https://doi.org/10.1007/s12975-021-00976-4>.

Acknowledgements This paper is dedicated to the memory of Professor Teng Ma, director of the cell and tissue engineering laboratory at FAMU-FSU College of Engineering, who suddenly passed away in May of 2019. S.C.G. acknowledges funding from NIH (RO1-NS102395). S.H. thanks NIH for financial support through a Ruth Kirschstein National Research Service Award (F31 NS115409).

Author Contribution All authors designed the study and critically revised and approved the final version of the manuscript. S.H. and F.A.B. contributed equally to this manuscript. S.H. performed surgeries with assistance from J.T.R. S.H. and F.A.B. performed behavioral assessment, MRI scans, data analysis, and statistical analysis and wrote the manuscript, with editing by S.C.G. X.Y. performed cell culture work under the supervision of T.M. K.X. and J.Y.L. performed histological assessment under the supervision of C.V.B. S.C.G., C.V.B., T.M., and J.T.R. conceived the project.

Funding S.C.G. acknowledges funding from NIH (RO1-NS102395). S.H. thanks NIH for financial support through a Ruth Kirschstein National Research Service Award (F31 NS115409). The National High Magnetic Field Laboratory is supported by the National Science Foundation through the NSF (DMR-1644779) and State of Florida.

Data Availability All data used in this study were newly acquired. Relevant data used in preparation of this manuscript are available upon request to either the principal or corresponding author via email. In accordance with the National High Magnetic Field Laboratory FAIR Data Management Plan (www.nationalmaglab.org/about/fair-data), data can be made available for access through the NHMFL publication database.

Declarations

Disclaimer The content is solely the responsibility of the authors and does not necessarily represent the official views of the National Institutes of Health.

Conflict of Interest Cesar Borlongan serves on the editorial board of Translational Stroke Research. All other authors report no conflicts of interest with respect to this work.

References

- Benjamin EJ, Blaha MJ, Chiuve SE, Cushman M, Das SR, Deo R, et al. Heart disease and stroke statistics—2017 update: a report from the American Heart Association. *Circulation*. 2017;135:e146–603. <https://doi.org/10.1161/CIR.0000000000000485>.
- National Institute of Neurological Disorders and Stroke rt-PA Stroke Study Group. Tissue plasminogen activator for acute ischemic stroke. *N Engl J Med*. 1995;333:1581–7.
- Hu H-J, Song M. Disrupted ionic homeostasis in ischemic stroke and new therapeutic targets. *J Stroke Cerebrovasc Dis*. 2017;26:2706–19. <https://doi.org/10.1016/j.jstrokecerebrovasdis.2017.09.011>.
- Madelin G, Lee J-S, Regatte RR, Jerschow A. Sodium MRI: methods and applications. *Prog Nucl Magn Reson Spectrosc*. 2014;79:14–47. <https://doi.org/10.1016/j.pnmrs.2014.02.001>.
- Boada FE, Qian Y, Nemoto E, Jovin T, Jungreis C, Jones SC, et al. Sodium MRI and the assessment of irreversible tissue damage during hyper-acute stroke. *Transl Stroke Res*. 2012;3:236–45. <https://doi.org/10.1007/s12975-012-0168-7>.
- Wey HY, Duong TQ. Multimodal MRI of nonhuman primate stroke. *Transl Stroke Res*. 2012;84–9.
- Wakabayashi K, Nagai A, Sheikh AM, Shiota Y, Narantuya D, Watanabe T, et al. Transplantation of human mesenchymal stem cells promotes functional improvement and increased expression of neurotrophic factors in a rat focal cerebral ischemia model. *J Neurosci Res*. 2009;88:NA-NA. <https://doi.org/10.1002/jnr.22279>
- Zacharek A, Chen J, Cui X, Li A, Li Y, Roberts C, et al. Angiopoietin1/Tie2 and VEGF/Flk1 induced by MSC treatment amplifies angiogenesis and vascular stabilization after stroke. *J Cereb Blood Flow Metab*. 2007;27:1684–91.
- Mora-Lee S, Sirerol-Piquer S, Gutiérrez-Pérez M, Gomez-Pinedo U, Roobrouck VD, Ló Pez T, et al. Therapeutic effects of hMAPC and hMSC transplantation after stroke in mice. *PLoS One*. 2012;7:e43683.
- Li Y, Chen J, Wang L, Lu M, Chopp M. Treatment of stroke in rat with intracarotid administration of marrow stromal cells. *Neurology*. 2001;56:1666–72.
- Horita Y, Honmou O, Harada K, Houkin K, Hamada H, Kocsis JD. Intravenous administration of glial cell line-derived neurotrophic factor gene-modified human mesenchymal stem cells protects against injury in a cerebral ischemia model in the adult rat. *J Neurosci Res*. 2006;84:1495–504.
- Chen J, Li Y, Wang Lei, Zhang Z, Lu D, Lu M, et al. Therapeutic benefit of intravenous administration of bone marrow stromal cells after cerebral ischemia in rats. *Stroke*. 2001;32:1005–11.
- Napoli E, Borlongan CV. Recent advances in stem cell-based therapeutics for stroke. *Transl Stroke Res*. 2016;7:452–7.
- Crigler L, Robey RC, Asawachaicharn A, Gaupp D, Phinney DG. Human mesenchymal stem cell subpopulations express a variety of neuro-regulatory molecules and promote neuronal cell survival and neurogenesis. *Exp Neurol*. 2006;198:54–64. <https://doi.org/10.1016/J.EXPNEUROL.2005.10.029>.
- Nomura T, Honmou O, Harada K, Houkin K, Hamada H, Kocsis JD. I.V. Infusion of brain-derived neurotrophic factor gene-modified human mesenchymal stem cells protects against injury in a cerebral ischemia model in adult rat. *Neuroscience*. 2005;136:161. <https://doi.org/10.1016/J.NEUROSCIENCE.2005.06.062>.
- Rowart P, Ericum P, Detry O, Weekers L, Grégoire C, Lechanteur C, et al. Mesenchymal stromal cell therapy in ischemia/reperfusion injury. *J Immunol Res*. 2015;2015:602597.
- NIH Search of: human mesenchymal stem cells | stroke - List Results - ClinicalTrials.gov.
- Copland IB, Galipeau J. Death and inflammation following somatic cell transplantation. *Semin Immunopathol*. 2011;33:535–50.
- Sart S, Liu Y, Ma T, Li Y. Microenvironment regulation of pluripotent stem cell-derived neural progenitor aggregates by human mesenchymal stem cell secretome. *Tissue Eng Part A*. 2014;20:2666–79.
- Teixeira FG, Carvalho MM, Sousa N, Salgado AJ. Mesenchymal stem cells secretome: a new paradigm for central nervous system regeneration? *Cell Mol Life Sci*. 2013.
- Tsai A-C, Liu Y, Yuan X, Ma T. Compaction, fusion, and functional activation of three-dimensional human mesenchymal stem cell aggregate. *Tissue Eng Part A*. 2015;21:1705–19. <https://doi.org/10.1089/ten.TEA.2014.0314>.
- Sart S, Tsai A-C, Li Y, Ma T. Three-dimensional aggregates of mesenchymal stem cells: cellular mechanisms, biological properties, and applications. *Tissue Eng Part B Rev*. 2014;20:365–80. <https://doi.org/10.1089/ten.TEB.2013.0537>.
- Guo L, Ge J, Zhou Y, Wang S, Zhao RCH, Wu Y. Three-dimensional spheroid-cultured mesenchymal stem cells devoid of embolism attenuate brain stroke injury after intra-arterial injection. *Stem Cells Dev*. 2014;23:978–89.
- Yuan X, Tsai A-C, Farrance I, Rowley JA, Ma T. Aggregation of culture expanded human mesenchymal stem cells in microcarrier-based bioreactor. *Biochem Eng J*. 2018;131:39–46. <https://doi.org/10.1016/j.bej.2017.12.011>.
- Tsai A-C, Liu Y, Yuan X, Chella R, Ma T. Aggregation kinetics of human mesenchymal stem cells under wave motion. *Biotechnol J*. 2017;12:1600448. <https://doi.org/10.1002/biot.201600448>.
- Bang OY, Moon GJ, Kim DH, Lee JH, Kim S, Son JP, et al. Stroke induces mesenchymal stem cell migration to infarcted brain areas via CXCR4 and C-met signaling the STARTING-2 trial investigators. *Transl Stroke Res*. 2017;8:449–60.
- Ramos-Cabrer P, Hoehn M. MRI stem cell tracking for therapy in experimental cerebral ischemia. *Transl Stroke Res*. 2012;3:22–35.
- Rosenberg JT, Sellgren KL, Sachi-Kocher A, Bejarano FC, Baird MA, Davidson MW, et al. Magnetic resonance contrast and biological effects of intracellular superparamagnetic iron oxides on human mesenchymal stem cells with long-term culture and hypoxic exposure. *Cytotherapy*. 2013;15:307–22.
- Naumova AV, Akulov AE, Khodanovich MY, Yarnykh VL. High-resolution three-dimensional macromolecular proton fraction mapping for quantitative neuroanatomical imaging of the rodent brain in ultra-high magnetic fields. *Neuroimage*. 2017;147:985–93.
- Yang Y, Salayandia VM, Thompson JF, Yang LY, Estrada EY, Yang Y. Attenuation of acute stroke injury in rat brain by minocycline promotes blood-brain barrier remodeling and alternative microglia/macrophage activation during recovery. *J Neuroinflammation*. 2015;12:26.
- He R, Moisan A, Detante O, Rémy C, Krainik A, Barbier EL, et al. Evaluation of parametric response mapping to assess therapeutic

- response to human mesenchymal stem cells after experimental stroke. *Cell Transplant*. 2017;26:1462–71.
32. Liu Y, Yuan X, Muñoz N, Logan TM, Ma T. Commitment to aerobic glycolysis sustains immunosuppression of human mesenchymal stem cells. *Stem Cells Transl Med*. 2018;8:93–106. <https://doi.org/10.1002/sctm.18-0070>.
 33. Longa EZ, Weinstein PR, Carlson S, Cummins R. Reversible middle cerebral artery occlusion without craniectomy in rats. *Stroke*. 1989;20:84–91.
 34. Tajiri N, Dailey T, Metcalf C, Mosley YI, Lau T, Staples M, et al. In vivo animal stroke models: a rationale for rodent and non-human primate models. *Transl Stroke Res*. 2013;4:308–21.
 35. Fu R, Brey WW, Shetty K, Gorōkov P, Saha S, Long JR, et al. Ultra-wide bore 900 MHz high-resolution NMR at the National High Magnetic Field Laboratory. *J Magn Reson*. 2005;177:1–8.
 36. Iglesias JE, Crampsie S, Strand C, Tachrount M, Thomas DL, Holton JL. Effect of Fluorinert on the Histological Properties of Formalin-Fixed Human Brain Tissue. *J Neuropathol Exp Neurol*. 2018;77:1085–90. <https://doi.org/10.1093/jnen/nly098>.
 37. Schaar KL, Brenneman MM, Savitz SI. Functional assessments in the rodent stroke model. *Exp Transl Stroke Med*. 2010;2:13. <https://doi.org/10.1186/2040-7378-2-13>.
 38. Schallert T, Fleming SM, Leasure JL, Tillerson JL, Bland ST. CNS plasticity and assessment of forelimb sensorimotor outcome in unilateral rat models of stroke, cortical ablation, parkinsonism and spinal cord injury. *Neuropharmacology*. 2000;39:777–87. [https://doi.org/10.1016/S0028-3908\(00\)00005-8](https://doi.org/10.1016/S0028-3908(00)00005-8).
 39. Pellow S, Chopin P, File SE, Briley M. Validation of open : closed arm entries in an elevated plus-maze as a measure of anxiety in the rat. *J Neurosci Methods*. 1985;14:149–67. [https://doi.org/10.1016/0165-0270\(85\)90031-7](https://doi.org/10.1016/0165-0270(85)90031-7).
 40. Crawley JN. Exploratory behavior models of anxiety in mice. *Neurosci Biobehav Rev*. 1985;9:37–44.
 41. Belzung C, Griebel G. Measuring normal and pathological anxiety-like behaviour in mice: a review. *Behav Brain Res*. 2001;125:141–9.
 42. Seibenhener ML, Wooten MC. Use of the open field maze to measure locomotor and anxiety-like behavior in mice. *J Vis Exp*. 2015;96:e52434.
 43. Yuan X, Rosenberg JT, Liu Y, Grant SC, Ma T. Aggregation of human mesenchymal stem cells enhances survival and efficacy in stroke treatment. *Cytotherapy*. 2019;21:1033–48. <https://doi.org/10.1016/j.jcyt.2019.04.055>.
 44. Sart S, Bejarano FC, Baird MA, Yan Y, Rosenberg JT, Ma T, et al. Intracellular labeling of mouse embryonic stem cell-derived neural progenitor aggregates with micron-sized particles of iron oxide. *Cytotherapy*. 2015;17:98–111.
 45. Imitola J, Raddassi K, Park KI, Mueller F-J, Nieto M, Teng YD, et al. Directed migration of neural stem cells to sites of CNS injury by the stromal cell-derived factor 1 α /CXCR4 chemokine receptor 4 pathway. *Proc Natl Acad Sci*. 2004;101:18117–22. <https://doi.org/10.1073/PNAS.0408258102>.
 46. Sart S, Ma T, Li Y. Preconditioning stem cells for *in vivo* delivery. *Biores Open Access*. 2014;3:137–49.
 47. Sofroniew MV, Vinters HV. Astrocytes: biology and pathology. *Acta Neuropathol*. 2010;119:7–35. <https://doi.org/10.1007/s00401-009-0619-8>.
 48. Vonderwalde I, Azimi A, Rolvink G, Ahlfors J-E, Shoichet MS, Morshead CM. Transplantation of directly reprogrammed human neural precursor cells following stroke promotes synaptogenesis and functional recovery. *Transl Stroke Res*. 2020;11:93–107. <https://doi.org/10.1007/s12975-019-0691-x>.
 49. Zimatkin SM, Karnyushko OA. Expression of doublecortin and neuron in developing neurons in the rat cerebellum. *Neurosci Behav Physiol*. 2017;47:122–6. <https://doi.org/10.1007/s11055-016-0374-y>.

Publisher's Note Springer Nature remains neutral with regard to jurisdictional claims in published maps and institutional affiliations.